First-principles study of hole trapping at GaSb/AlSb heterointerfaces: Unveiling the role of orbital hybridization in Al-related defects

Jia-Yi Yuan(袁嘉怡)[1,2], Zhu-You Liu(刘竹友)[1], Cai-Xin Zhang(张才鑫)[1], Yue-Yang Liu(刘岳阳)[1], Chen Zhang(张陈)[1,2,†], and Hui-Xiong Deng(邓惠雄)[1,2,‡]

[1] *State Key Laboratory of Semiconductor Chip Physics and Technology, Institute of Semiconductors, Chinese Academy of Sciences (CAS), Beijing* 100083, *China*

[2] *Center of Materials Science and Optoelectronics Engineering, University of Chinese Academy of Sciences, Beijing* 100049, *China*

(Received 5 September 2025; revised manuscript received 17 October 2025; accepted manuscript online 13 November 2025)

Antimony-based (Sb-based) short-wave infrared (SWIR) photodetectors have attracted considerable attention for their applications in non-destructive optical analysis. However, defect-induced charge trapping at heterojunction interfaces severely degrades device performance and stability, while the dominant defect types and their underlying physical mechanisms remain poorly understood. In this study, we employ first-principles calculations with Marcus charge transfer theory to investigate the defect-induced hole trapping process within the GaSb/AlSb heterojunction. We find that among all intrinsic defects examined, Sb vacancy (V_{Sb}), Al vacancy (V_{Al}), and the Al antisite on Sb (Al_{Sb}) introduce shallow acceptor levels near the valence band maximum (VBM), rendering them highly effective in trapping holes. Moreover, we demonstrate that Al-related defects (V_{Al} and Al_{Sb}) undergo substantial orbital hybridization with the VBM. This significantly enhances the coupling strength between the initial and final states, thereby boosting hole trapping efficiency. These findings provide crucial insights into the performance limitations of Sb-based SWIR photodetectors and offer valuable guidance for defect engineering and device optimization.

Keywords: hole trapping, interface defects, orbital hybridization, first-principles study

PACS: 72.20.Jv, 71.55.–i, 73.40.Kp

DOI: 10.1088/1674-1056/ae1f00 **CSTR:** 32038.14.CPB.ae1f00

1. Introduction

Short-wave infrared (SWIR) photodetectors, operating within the atmospheric window of 1 μm–3 μm, uniquely combine long-range detection and high-resolution imaging capabilities.[1,2] This enables critical applications in many fields, such as autonomous driving,[3–5] satellite surveying,[6,7] *etc*. For the SWIR detector material systems, many have been studied, including Si-based,[8–10] HgCdTe,[11,12] graphene,[13,14] InGaAs,[15–17] and Sb-based detectors.[18–20] Among these, Sb-based InAs/GaSb/AlSb type-II superlattice detectors stand out as a leading "third-generation" candidate, addressing the critical limitations of established technologies, such as the lattice mismatch in InGaAs and the high cost and poor uniformity of HgCdTe.[21] A key innovation in this material family is the incorporation of wide-bandgap AlSb layers, which enables advanced band-structure engineering to achieve wide spectral tunability without strain, while maintaining the superior epitaxial quality required for large-area substrates.[22–24]

However, the performance and stability of Sb-based SWIR detectors are often limited by charge trapping.[24,25] As a critical source of instability common to many infrared photodetector systems, charge trapping is well documented to induce multiple deleterious effects, including degraded photometric precision, interfacial charge accumulation, enhanced carrier recombination, and the introduction of spurious time-dependent signals.[26–28] Current performance studies of Sb-based SWIR photodetectors predominantly focus on macroscopic characteristics, such as dark current, with the analyses being closely integrated with experimental data. A typical example is the widely adopted Shockley model, which incorporates physical parameters determined via experimental techniques: doping concentration is commonly extracted through capacitance–voltage (C–V) profiling, carrier diffusion lengths can be derived from Hall measurements, and the generation–recombination (GR) lifetimes (τ_{GR}) are determined by fitting the model to measured current–voltage curves.[24,25] However, the underlying microscopic physics, specifically the charge trapping mechanisms that dictate these capture rates and dark current, remains unclear.

To address these issues, in this study, we employ first-principles calculations to investigate hole trapping by intrinsic defects at the GaSb/AlSb interface, a critical process in

†Corresponding author. E-mail: zhangchen192@semi.ac.cn

‡Corresponding author. E-mail: hxdeng@semi.ac.cn

© 2026 Chinese Physical Society and IOP Publishing Ltd. All rights, including for text and data mining, AI training, and similar technologies, are reserved.

CPB Online In Press

devices where GaSb serves as the primary hole potential well.[29–31] We compare the hole trapping rates of all considered defects, identifying Al-related defects (V_{Al} and Al_{Sb}) as exceptionally efficient hole trapping centers with trapping rates reaching up to 10^{14} s^{-1}. More importantly, we find that the physical origin of enhanced hole trapping arises from strong orbital hybridization between Al-related defects and valence band maximum (VBM) states. Our results provide fundamental *ab initio* insights into carrier trapping mechanisms in Sb-based SWIR, and offer valuable guidance for strategic defect engineering and device optimization.

2. Methods

2.1. DFT calculations

All density functional theory (DFT) calculations are performed using the plane-wave package PWmat with graphics processing unit acceleration.[32,33] In all calculations, we adopt the SG15 norm-conserving pseudopotentials and an energy cutoff of 50 Ry for the basis set. For structural relaxations, we employ the Perdew–Burke–Ernzerhof (PBE) functional, and the convergence criterion is set to 0.02 eV/Å for the maximum Hellmann–Feynman force on each atom. For electronic structure calculations, we maintain the same computational parameters but employ the Heyd–Scuseria–Ernzerhof (HSE06) hybrid functional with atom-weighted mixing parameters to accurately describe the band structures and band offsets of GaSb and AlSb.[34] This method enables continuous bandgap tuning through adjustment of the a_i and σ_i parameters.[35] Using parameter sets of ($a_i = -0.20$, $\sigma_i = 2.75$) for GaSb and ($a_i = -0.29$, $\sigma_i = 2.75$) for AlSb, we obtained bandgaps of 0.78 eV and 1.62 eV, respectively, showing excellent agreement with experimental values.[23]

Furthermore, we constructed the GaSb(100)/AlSb(100) heterojunction using the interface builder tool in Quantum ATK.[36] The GaSb(100)/AlSb(100) heterojunction is built with Sb atoms serving as the common interface atoms, while a uniform strain below 5% was applied to the AlSb layer to accommodate the slight lattice mismatch between the two materials. In addition, a vacuum layer of approximately 20 Å is added in the direction perpendicular to the interface. The resulting heterostructure supercell, with dimensions of 12.33 Å×12.33 Å×65.76 Å, consists of 8 Ga layers, 8 Al layers, and 15 Sb layers, totaling 280 atoms. All exposed Ga and Al dangling bonds on both sides of the heterojunction are passivated with pseudo-hydrogen atoms. The reliability of this supercell size is validated by convergence tests on key defect properties and by its favorable comparison to dimensions used in similar first-principles studies of interface charge trapping.[37,38]

2.2. Marcus theory

To further investigate the charge trapping caused by interfacial defects, we calculated the hole trapping rates using Marcus charge transfer theory.[39,40] The charge trapping rate is given by

$$\nu = \frac{2\pi}{\hbar}|V_c|^2\sqrt{\frac{1}{4\pi\lambda k_B T}}\exp\left[-\frac{(\Delta G+\lambda)^2}{4\lambda k_B T}\right], \tag{1}$$

where ΔG represents the Gibbs free energy difference between the initial and final states for the charge transfer reaction, λ is the reorganization energy of structural relaxation during charge trapping, and V_c is the coupling constant between the initial and final states.[41] In practice, we calculate V_c by using an electric field to intentionally drive the two-level system (*e.g.*, VBM and defect level) into a crossing region, where an anti-crossing behavior occurs, and V_c is exactly half of the anti-crossing energy gap.[37] In our calculations, the external electric field was modeled as a linear potential applied perpendicular to the heterointerface. This strategy has been successfully demonstrated for charge transfer dynamics at different interfacial systems.[37,38,41–43]

Furthermore, when Sb-based SWIR photodetectors are in operation, an external electric field is often applied to efficiently separate photogenerated electron–hole pairs.[24,25] The applied electric field F will change the position of the defect level relative to the VBM, which is reflected in modifying the Gibbs free energy as

$$\Delta G(F) = \Delta G_0 - eFd. \tag{2}$$

Here, ΔG_0 is the Gibbs free energy difference in the absence of an electric field, e is the elementary charge, and d is the defect-interface distance.[37,38] By substituting ΔG with $\Delta G(F)$, the effect of the external electric field can be incorporated.

3. Results and discussion

The GaSb/AlSb heterojunction is constructed by epitaxial connection of the GaSb(100) and AlSb(100) surfaces, where Sb atoms naturally bridge the interface [Fig. 1(a)]. At this interface, both Ga and Al atoms retain their tetrahedral coordination, forming Ga–Sb–Al bonding configurations. During structural relaxation, we fix the outermost five layers of each material to preserve their bulk properties. The relaxed structure reveals minimal bond distortion, with the interfacial Ga–Sb and Al–Sb bonds both converging to 2.67 Å. While GaSb and AlSb exhibit T_d symmetry in their bulk forms, the point group symmetry of the GaSb/AlSb heterojunction is reduced to C_{2v}, as the symmetry in the z-direction is broken, while the xy-plane remains almost unaffected. For the purpose of analysis, we sequentially label six distinct positions with increasing distance d from the shared Sb layer, three within the interface (I-1, I-2, I-3) and three within the bulk (B-4, B-5, B-6). At each designated position, a defect can be introduced on either

CPB Online In Press

an Al or an Sb atomic site. Figure 1(a) highlights the interface and bulk regions where a defect can be placed.

Furthermore, we determine the band offset between GaSb and AlSb by aligning the macroscopic averaged potentials. The GaSb/AlSb heterojunction forms a type-II band alignment, with the valence band offset (VBO) and conduction band offset (CBO) of AlSb relative to GaSb determined to be 0.38 eV and 0.46 eV, respectively [Fig. 1(c)]. These values exhibit good agreement with previously reported experimental and theoretical data,[23,44,45] which validates the accuracy of our calculated electronic structures. Further orbital analysis of the heterojunction band edge states reveals that the CBM is primarily composed of Ga-4s and Sb-5s orbitals, with minor contributions from Sb-5p_z and Ga-4p_z. The VBM, in contrast, consists mainly of Sb-5p_x and Sb-5p_y orbitals. This distinct orbital composition stems from C_{2v} point group symmetry of the heterojunction. As illustrated in Fig. 1(b), the s and p_z orbitals from both Ga and Sb atoms couple under the same symmetry representation and form the CBM state, whereas the p_x and p_y orbitals form the bonding states that constitute the VBM.

To investigate hole trapping effects within the GaSb/AlSb heterojunction, we perform first-principles calculations on six intrinsic defects in AlSb: Sb vacancy (V_{Sb}), Al vacancy (V_{Al}), Al antisite on Sb (Al_{Sb}), Sb antisite on Al (Sb_{Al}), Al interstitial (Al_i) and Sb interstitial (Sb_i). For each defect type, we examine six previously defined positions to evaluate distance-dependent trapping behavior. The calculated defect energy levels for these intrinsic defects, all corresponding to their neutral charge state, shown in Fig. 1(c), reveal that Sb_{Al}, Al_i, and Sb_i display deep acceptor levels. According to Marcus theory, these deep acceptor levels imply high charge transfer energy barriers and low hole trapping efficiency. However, V_{Al}, V_{Sb}, and Al_{Sb} introduce shallow acceptor levels near the heterojunction VBM. The origin of these shallow defect levels varies significantly: (i) V_{Al} forms a conventional shallow acceptor level near the VBM, originating from Sb-5p_x/p_y orbitals of broken Al–Sb bonds; (ii) surprisingly, V_{Sb} also creates a shallow acceptor level, despite expectations that the Al-3p orbital contribution would position it near the CBM. This anomaly stems from significant structural relaxation. Due to the large Al/Sb size mismatch, an internal strain is generated, causing the four surrounding Al atoms to move towards the vacancy center. Specifically, the Al–Al distance decreases by approximately 30%. This deformation causes the defect electrons to be strongly attracted to the positive Al nuclei, which drastically lowers the defect energy level into a shallow acceptor state; (iii) while for Al_{Sb}, the Al atom occupying an Sb site introduces Al–Al orbital coupling, resulting in shallow bonding states primarily composed of Al-3p_x/p_y orbitals. These shallow acceptor levels render them more efficient for hole trapping. Consequently, we focus subsequent hole trapping efficiency calculations specifically on these three V_{Sb}, V_{Al}, and Al_{Sb} defects.

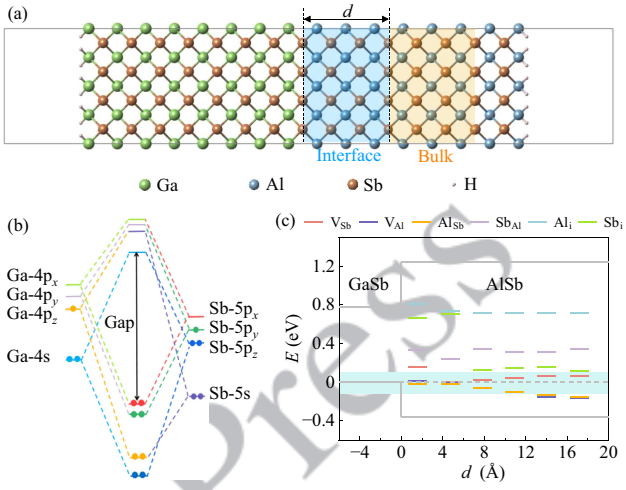


Fig. 1. (a) Atomic structure of GaSb/AlSb heterojunction. The blue and orange shaded areas highlight the interface and bulk regions within the AlSb side, respectively, which contain the designated positions for point defect analysis. The variable d denotes the distance from the shared Sb interface. (b) Schematic diagram of atomic orbital coupling in GaSb. Solid dots on the energy levels denote electron occupation. (c) Calculated defect levels for intrinsic defects in AlSb at the six designated atomic sites. The shaded area distinguishes shallow defects. All defect levels shown correspond to the neutral charge state of the defects.

Furthermore, we show in Fig. 2 the reorganization energies λ and coupling constants V_c of V_{Sb}, V_{Al}, and Al_{Sb} for the hole trapping dynamics. While all three defects exhibit comparable reorganization energies in the range of 0–12 meV, their coupling constants display significant variations. Notably, V_{Al} and Al_{Sb} demonstrate coupling constants approximately one order of magnitude larger than V_{Sb}. This distinction arises from fundamental differences in orbital contributions, as the defect levels of V_{Al} and Al_{Sb} primarily derive from p_x/p_y orbitals, which exhibit strong wavefunction overlap with the VBM due to their similar orbital character. In contrast, the V_{Sb} defect level contains significant s and p_z orbital contributions, resulting in weaker overlap with the VBM. Furthermore, we observed that the coupling constants for all three defects follow an exponential decay with increasing distance from the interface. This behavior reflects the expected reduction in wavefunction overlap as defects move further into the bulk region.

Based on these physical quantities, we calculate the hole trapping rate of these defects at different atomic sites under different applied electric fields, and the results are shown in Fig. 3. Here, we define the positive direction of the electric field as pointing from the GaSb layer to the AlSb layer. Without an external electric field, the maximum hole trapping rate of the V_{Sb}, V_{Al}, and Al_{Sb} is about 10^{11}, 10^{13}, and 10^{14} s^{-1}, respectively. This renders the V_{Al} and Al_{Sb} defects as the major hole-trapping centers, while the V_{Sb} defect makes a limited contribution. This is consistent with our

CPB Online in Press

analysis of the coupling constants above. Furthermore, since the defects closer to the interface have larger coupling constants, the interfacial defects exhibit a significantly larger hole trapping rate compared to their bulk counterparts. Moreover, for most defects, we observe that as the applied electric field increases, the hole trapping rate initially increases and then decreases. This behavior is a manifestation of the Marcus-inverted charge transfer phenomenon,[46,47] a universal kinetic model essential for understanding charge dynamics in systems ranging from molecular chemistry to advanced semiconductor heterostructures.[48–51] In our system, this non-monotonic trend can be understood as follows: as the applied electric field increases, the defect level, which is initially slightly above the GaSb VBM, gradually approaches the GaSb VBM, thereby reducing the hole transfer energy barrier and increasing the hole trapping rate. However, with further increases in the applied electric field, the defect energy level begins to fall below the GaSb VBM. At this point, the energy difference between them then reversely increases with the field, which, in turn, raises the hole transfer energy barrier and decreases the hole trapping rate.

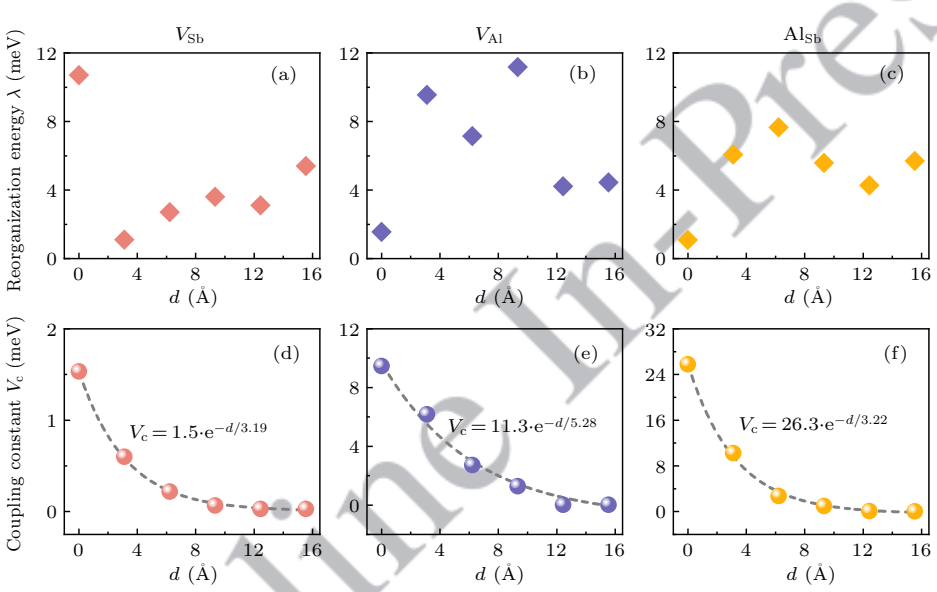


Fig. 2. (a)–(c) Reorganization energy λ and (d)–(f) coupling constant V_c calculated at different atomic sites for V_{Sb} (red), V_{Al} (purple), and Al_{Sb} (yellow) defects in AlSb.

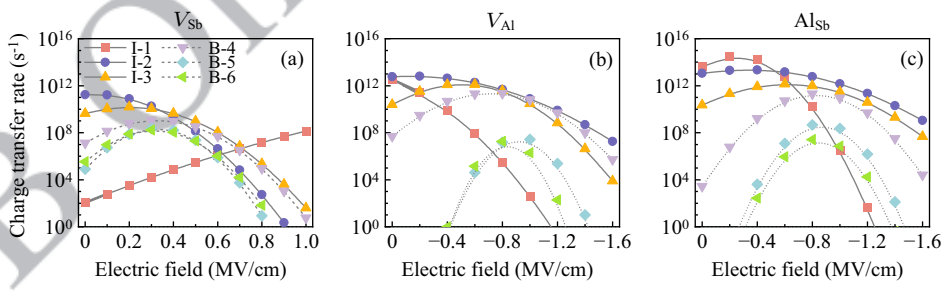


Fig. 3. Hole trapping rate under applied electric field at different atomic sites of (a) V_{Sb}, (b) V_{Al}, and (c) Al_{Sb} defects in AlSb. The common legend applies to all subplots, where solid and dashed lines represent interface and bulk defects, respectively.

4. Conclusion

This work employs first-principles calculations and Marcus charge transfer theory to investigate the microscopic mechanisms of hole trapping by intrinsic defects at the GaSb/AlSb heterointerface, a critical process which limits the performance of Sb-based SWIR photodetectors. Our results identify the Al-related defects, namely Al vacancy (V_{Al}) and Al antisite on Sb (Al_{Sb}), as the primary hole trapping centers. Their exceptional efficiency is attributed to the synergy of two distinct factors: a low hole transfer energy barrier provided by their shallow acceptor levels, and a large electronic coupling constant resulting from strong orbital hybridization with the VBM states. The combination of energetic and kinetic advantages leads to hole trapping rates orders of magnitude greater than other defects like Sb vacancy (V_{Sb}), an effect most pronounced near the interface where greater wavefunction overlap maximizes the electronic coupling. These studies offer a crucial, atomistic-level insight beyond previous macroscopic models and provide direct guidance for targeted defect engineering to enhance performance and stability in next-generation Sb-based infrared photodetectors.

CPB Online In Press

Acknowledgements

Project supported by the Strategic Priority Research Program of the Chinese Academy of Sciences (Grant No. XDB0460000), the National Natural Science Foundation of China (Grant No. 62425406), the National Key Research and Development Program of China (Grant No. 2024YFA1409700), the CAS Project for Young Scientists in Basic Research (Grant No. YSBR-026), the Youth Innovation Promotion Association of the Chinese Academy of Sciences (Grant No. Y2021042).

References

[1] Guan X, Yu X, Periyanagounder D, Benzigar M R, Huang J K, Lin C H, Kim J, Singh S, Hu L, Liu G, Li D, He J H, Yan F, Wang Q J and Wu T 2021 *Adv. Opt. Mater.* **9** 2001708
[2] Wu Z, Ou Y, Cai M, Wang Y, Tang R and Xia Y 2023 *Adv. Opt. Mater.* **11** 2201577
[3] Pavlović M S, Milanović P D, Stanković M S, Perić D B, Popadić I V and Perić M V 2022 *Sensors* **22** 2562
[4] Li Y, Moreau J and Ibanez-Guzman J 2023 *IEEE Trans. Intell. Transp. Syst.* **24** 4716
[5] Valme D, Rassõlkin A and Liyanage D C 2025 *Sensors* **25** 2346
[6] Park H and Choi J 2021 *Sustainability* **13** 5518
[7] Koerting F, Asadzadeh S, Hildebrand J C, Savinova E, Kouzeli E, Nikolakopoulos K, Lindblom D, Koellner N, Buckley S J, Lehman M, Schläpfer D and Micklethwaite S 2024 *Mining* **4** 1013
[8] Katiyar A K, Thai K Y, Yun W S, Lee J and Ahn J H 2020 *Sci. Adv.* **6** eabb0576
[9] Ahmad H, Thambiratnam K, Leong T C, Thandavam T M K and Ramli R 2019 *IEEE 9th International Nanoelectronics Conferences (INEC)*, July 2019, pp. 1–3
[10] Cong H, Xue C, Zheng J, Yang F, Yu K, Liu Z, Zhang X, Cheng B and Wang Q 2016 *IEEE Photon. J.* **8** 1
[11] Bubulac L O, Tennant W E, Pasko J G, Kozlowski L J, Zandian M, Motamedi M E, De Wames R E, Bajaj J, Nayar N, McLevige W V, Gluck N S, Melendes R, Cooper D E, Edwall D D, Arias J M, Hall R and D'souza A I 1997 *J. Electron. Mater.* **26** 649
[12] Cervera C, Boulade O, Gravrand O, Lobre C, Guellec F, Sanson E, Ballet P, Santailler J L, Moreau V, Zanatta J P, Fieque B and Castelein P 2017 *J. Electron. Mater.* **46** 6142
[13] Zhang B Y, Liu T, Meng B, Li X, Liang G, Hu X and Wang Q J 2013 *Nat. Commun.* **4** 1811
[14] Chen Z, Li X, Wang J, Tao L, Long M, Liang S J, Ang L K, Shu C, Tsang H K and Xu J B 2017 *ACS Nano* **11** 430
[15] Arslan Y, Oguz F and Besikci C 2015 *Infrared Phys. & Technol.* **70** 134
[16] Manda S, Matsumoto R, Saito S, Maruyama S, Minari H, Hirano T, Takachi T, Fujii N, Yamamoto Y, Zaizen Y, Hirano T and Iwamoto H 2019 *IEEE International Electron Devices Meeting (IEDM)*, December 2019, pp. 16.7.1–16.7.4
[17] Yuan H, Zhang J, Kim J, Bond D, Laquindanum J, Kimchi J and DeForest M G 2019 *Infrared Sensors, Devices, and Applications IX* (Proc. SPIE 11129) 111290E
[18] Razeghi M, Dehzangi A and Li J 2021 *Results Opt.* **2** 100054
[19] Razeghi M 2020 *Infrared Technology and Applications XLVI* (Proc. SPIE 11407) 114070T
[20] Hussain L, Pettersson H, Wang Q, Karim A, Anderson J, Jafari M, Song J, Choi W J, Han I K and Lim J Y 2018 *J. Korean Phys. Soc.* **73** 1604
[21] Jiang J, Chang F, Zhou W, Li N, Chen W, Jiang D, Hao H, Wang G, Wu D, Xu Y and Niu Z C 2023 *Chin. Phys. B* **32** 038503
[22] Nguyen B M, Hoffman D, Delaunay P Y, Huang E K W, Razeghi M and Pellegrino J 2008 *Appl. Phys. Lett.* **93** 163502
[23] Kroemer H 2004 *Physica E* **20** 196
[24] Xie R, Li N, Shan Y, Su X, Zhou W, Chang F, Liang Y, Jiang D, Wang G, Hao H, Xu Y, Wu D and Niu Z 2024 *Infrared Phys. & Technol.* **136** 105074
[25] Li M, Cheng Y, Zhang X, Zhang Y, Jiang D, Song Z and Zheng W 2024 *AIP Adv.* **14** 095305
[26] Rousset H, Baier N, Sam-Giao D, Le Goff T, Nicolas J A and Gravrand O 2025 *J. Electron. Mater.* **54** 8350
[27] Grosman A, Manis Levy H and Sarsui G 2021 *J. Appl. Phys.* **129** 214504
[28] Qiao H, Hu W D, Ye Z H, Li X Y and Gong H M 2010 *J. Semicond.* **31** 036003
[29] Zakharova A, Yen S T and Chao K A 2001 *Phys. Rev. B* **64** 235332
[30] Kolek A 2023 *Phys. Rev. Appl.* **19** 024059
[31] Manyk T, Hackiewicz K, Rutkowski J and Martyniuk P 2018 *J. Semicond.* **39** 094004
[32] Jia W, Fu J, Cao Z, Wang L, Chi X, Gao W and Wang L W 2013 *J. Comput. Phys.* **251** 102
[33] Jia W, Cao Z, Wang L, Fu J, Chi X, Gao W and Wang L W 2013 *Comput. Phys. Commun.* **184** 9
[34] Heyd J and Scuseria G E 2004 *J. Chem. Phys.* **121** 1187
[35] Zheng F, Pham H H and Wang L W 2017 *Phys. Chem. Chem. Phys.* **19** 32617
[36] Smidstrup S, Markussen T, Vancraeyveld P, Wellendorff J, Schneider J, Gunst T, Verstichel B, Stradi D, Khomyakov P A, Vej-Hansen U G, Lee M E, Chill S T, Rasmussen F, Penazzi G, Corsetti F, Ojanperä A, Jensen K, Palsgaard M L N, Martinez U, Blom A, Brandbyge M and Stokbro K 2020 *J. Phys.: Condens. Matter* **32** 015901
[37] Liu Y Y, Liu F, Wang R, Luo J W, Jiang X, Huang R, Li S S and Wang L W 2019 *Phys. Rev. Appl.* **12** 064012
[38] Liu Z Y, Cai X, Zhang C X, Cao R Y, Liu Y Y and Deng H X 2023 *J. Phys. D: Appl. Phys.* **56** 105101
[39] Marcus R A 1965 *J. Chem. Phys.* **43** 679
[40] Marcus R A 1956 *J. Chem. Phys.* **24** 966
[41] Liu Y Y, Zheng F, Jiang X, Luo J W, Li S S and Wang L W 2019 *Phys. Rev. Appl.* **11** 044058
[42] Ma X, Liu Y Y, Zeng L, Chen J, Wang R, Wang L W, Wu Y and Jiang X 2022 *ACS Appl. Mater. Interfaces* **14** 2185
[43] Tarafder K, Surendranath Y, Olshansky J H, Alivisatos A P and Wang L W 2014 *J. Am. Chem. Soc.* **136** 5121
[44] Gualtieri G J, Schwartz G P, Nuzzo R G and Sunder W A 1986 *Appl. Phys. Lett.* **49** 1037
[45] Longenbach K F, Luo L F and Wang W I 1990 *Appl. Phys. Lett.* **57** 1554
[46] Closs G L, Calcaterra L T, Green N J, Penfield K W and Miller J R 1986 *J. Phys. Chem.* **90** 3673
[47] Grampp G 1993 *Angew. Chem. Int. Ed.* **32** 691
[48] Parada G A, Goldsmith Z K, Kolmar S, Pettersson Rimgard B, Mercado B Q, Hammarström L, Hammes-Schiffer S and Mayer J M 2019 *Science* **364** 471
[49] Chan A Y, Ghosh A, Yarranton J T, Twilton J, Jin J, Arias-Rotondo D M, Sakai H A, McCusker J K and MacMillan D W C 2023 *Science* **382** 191
[50] Wang J, Ding T, Gao K, Wang L, Zhou P and Wu K 2021 *Nat. Commun.* **12** 6333
[51] Xi Z 2025 *RSC Adv.* **15** 26897

Chin. Phys. B In Press